High-Frequency Current-Controlled Vortex Oscillations in Ferrimagnetic Disks

C.E. Zaspel,[1,*] E.G. Galkina,[2] and B.A. Ivanov[3,4,5]

[1] *Department of Environmental Sciences, University of Montana-Western, Dillon, Montana 59725, USA*
[2] *Institute of Physics, National Academy of Science of Ukraine, 03142 Kiev, Ukraine*
[3] *Institute of Magnetism, National Academy of Science of Ukraine, 03142 Kiev, Ukraine*
[4] *National University of Science and Technology "MISiS", Moscow 119049, Russian Federation*
[5] *Faculty of Radio Physics, Electronics and Computer Systems, Taras Shevchenko National University, Kiev 01601, Ukraine*

(Received 26 June 2019; revised manuscript received 9 September 2019; published 9 October 2019)

Recently, it has been shown that ferrimagnets made from Gd(Fe, Co) alloys exhibit ultrafast dynamics near the angular momentum compensation point. Owing to the small net magnetization in these alloys, stable magnetic vortices can be the ground state in a nanoscale disk, and gyrotropic motion can be driven by spin torque. It is shown that the Oersted field from the current can stabilize the vortex, and the critical current for gyrotropic motion and the current-dependent frequency are calculated in the Thiele model. This system can be used as a vortex-state spin-torque auto-oscillator working at frequencies of tens of gigahertz.

DOI: 10.1103/PhysRevApplied.12.044019

I. INTRODUCTION

In the search for higher frequency ranges of magnetic-vortex-based nanopillar oscillators, it is shown [1] that ferrimagnetic disks made with rare earth-transition metal alloys at the compensation point have gyrotropic frequencies much higher than those of ferromagnets. However, when used in spin-torque oscillator applications, there is a serious limitation, namely, for ferrimagnetic [1] and antiferromagnetic [2] vortices, the critical size of the disk is much larger than that of the standard permalloy disk size. In particular, the large value of the critical thickness limits the possibility of using ferrimagnetic vortices as spin-torque generators (for spintronic applications, thin free layers less than 5 nm are required). Here, it is shown that these limitations can be overcome through the Oersted field from a current perpendicular to the free layer in a typical nanopillar; this will tend to stabilize the vortex at smaller thicknesses. In addition, the current will also significantly increase the frequency-tuning range relative to that of ferromagnetic spin-torque oscillators.

In addition to nano-oscillators [3–6], the magnetic vortex structure makes these systems useful in areas such as information storage [7–9] and logic gates [10]. For microwave frequency oscillator applications, the vortices in ferromagnetic disks can exhibit high-amplitude sub-GHz gyrotropic oscillation of the vortex core about the disk center; this makes them particularly useful as microwave signal generators. In vortex oscillators driven by spin torque, the restoring force [11] controls the oscillation frequency. Two contributions to the restoring force are magnetostatic, arising from the formation of magnetostatic charge, as the vortex is displaced from the disk center and the Oersted field from an electron current in the nanopillar device. Therefore, the frequency is determined by the saturation magnetization and the disk aspect ratio, L/R, for a disk of radius R and thickness L. An advantage of vortex-state spin-torque oscillators is the uniquely narrow generated line width and high amplitude compared with that of nanopillar devices based on magnets with quasi-uniform magnetizations [3,4,6,11]. However, there are two disadvantages of ferromagnetic spin-torque vortex oscillators: the frequency is limited to about 1–2 GHz, which is only tunable through variation of the electron current, and a slight frequency variation through the corresponding Oersted field [12] from a current perpendicular to the disk.

To exploit the high amplitude of vortex oscillations, as well as the ultrafast vortex oscillations in transition metal-rare earth alloys [1,13], it is necessary to show that ferrimagnetic vortices are supported in disks thin enough for spin-torque applications. In the following, it is demonstrated that an Oersted field from a current perpendicular to the free layer in a typical nanopillar driven by spin torque will tend to stabilize the vortex for a smaller free-layer thickness. Moreover, it is shown how a spin-polarized current will excite high-frequency orbital motion of the vortex core, and the Oersted energy significantly increases the tunable frequency range of vortex-based spin-torque

*craig.zaspel@umwestern.edu

oscillators. The design of this spin-torque oscillator can be the same as that for the standard vortex-state oscillators based on a spin-valve nanopillar made with metallic ferromagnets, where giant magnetoresistance (GMR) is the source of an ac signal. Conceptually, the simplest system is a magnetic nanopillar with three magnetic layers [14,15], where the vortex precession in a soft magnetic layer is excited by spin-polarized current through the polarizer (see Fig. 1 and the discussion in the Sec. II). In this system, vortex precession leads to the rotation of total sublattice spins in the plane of the soft layer. The ac signal is produced by the GMR effect in the contact of the soft layer and analyzer with in-plane magnetization. For ferromagnetic bilayer systems, the contribution of GMR to the resistivity of the contact "soft layer-analyzer" with the magnetic moments $\vec{M}_{\rm soft}$ and $\vec{M}_{\rm an}$ depends on the mutual orientation of these moments, $\Delta\rho \propto (\vec{M}_{\rm soft} \cdot \vec{M}_{\rm an})$. Equivalently, the standard bilayer system, where the GMR signal is created on a free-layer contact with the polarizer, could be used, but the polarizer magnetization should be inclined to the disk normal.

For two sublattice magnets, the total conductivity is the sum of two partial conductivities caused by two sublattices. Since the magnetic sublattices in ferrimagnets are formed by different magnetic ions, their partial conductivities are different. This property was reported recently [16], where a wide range of magnetoresistive effects in ferrimagnetic Gd(Fe, Co) wre investigated. The magnetic moment

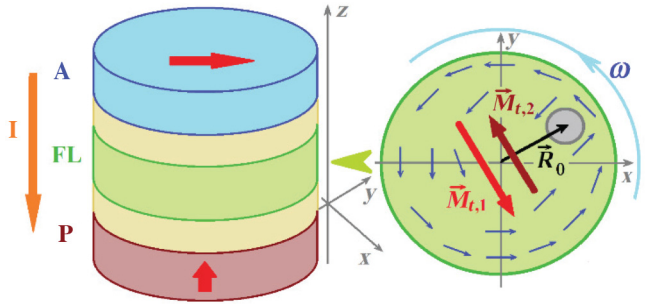

FIG. 1. Sketch of a three-layered magnetic nanostructure (schematically). Left: three-layer nanopillar structure as in Ref. [14]. P denotes the polarizer; FL is the free ferrimagnetic layer in the vortex state; and A: denotes the analyzer; layers of nonmagnetic metals are shown between them. The long orange arrow indicates the direction of the current (antiparallel to the direction of the electron flow), and the thick red arrows indicate the direction of magnetization in the polarizer and in the analyzer. Right: the instant directions of the total magnetic moments of transition-metal spins, $\vec{M}_{t,1} = \int \vec{M}_1(\vec{r},t)d^2r$, and rare-earth spins, $\vec{M}_{t,2} = \int \vec{M}_2(\vec{r},t)d^2r$. The vectors $\vec{M}_{t,1}$ and $\vec{M}_{t,2}$ are perpendicular to the displacement of the vortex core from the origin by $\vec{R}_0(t)$; these vectors are rotating with frequency ω. Thin blue arrows show schematically the direction of the antiferromagnetic vector $\vec{l}$, which is proportional to the difference of the sublattice spin densities, see the text for details.

of transition-metal subsystem Fe-Co is solely responsible for the magnetoresistance, and all effects show monotonic behavior across the compensation point [16]. Thus, one can expect a nonsmall GMR signal for the ferromagnet-ferrimagnet spin-valve nanopillar, even near the compensation point, which is similar to a standard ferromagnetic system. Unfortunately, we are unable to find any references in the literature for GMR in ferrimagnet-transition layer contacts. Notably, for antiferromagnets, the situation is completely different: the magnetic sublattices in antiferromagnet are formed by identical atoms; therefore, the partial conductivities of spin-polarized electrons are equal, and one can expect an absence of the GMR effects in a ferromagnet-antiferromagnet spin-valve structure [17].

II. FERRIMAGNETIC VORTEX DYNAMICS

To investigate the dynamics of the ferrimagnetic vortex, we begin with the two-sublattice model with magnetizations $\vec{M}_{1,2}$. These magnetizations are related to the spin-volume densities $\vec{s}_{1,2}$ by $\vec{M}_{1,2} = g_{1,2}\mu_B\vec{s}_{1,2}$, where g_1 and g_2 are the sublattice g values and μ_B is the Bohr magneton. At the angular momentum compensation point, $s_1 = s_2$ (here and below $s_{1,2} = |\vec{s}_{1,2}|$), it is convenient to use the antiferromagnetic two-sublattice formulation for the spin densities, $\vec{m} = (\vec{s}_1 + \vec{s}_2)/(s_1 + s_2)$ and $\vec{l} = (\vec{s}_1 - \vec{s}_2)/(s_1 + s_2)$. In the linear approximation on the small parameter $s_1 - s_2$, they are constrained as $\vec{m} \cdot \vec{l} = (s_1 - s_2)/(s_1 + s_2)$ and $\vec{m}^2 + \vec{l}^2 = 1$. Transforming from a discrete to a continuum model, the energy density can then be expressed as

$$w = \frac{E_{\rm ex}}{2}\vec{m}^2 + \frac{A}{2}(\nabla\vec{l})^2 - \frac{\mu_0\vec{M}}{2}(\vec{B}_{\rm MS} + 2\vec{B}_{\rm Oe}). \quad (1)$$

Here, first two terms are the standard forms of the exchange energy for the two sublattice magnets, such as ferrimagnets or antiferromagnets [1,13,18–22]; $E_{\rm ex}$ is the homogeneous exchange energy; and A is the nonhomogeneous exchange constant, reflecting the structure of magnetic excitations. Their values for the material of interest, Gd(Fe, Co) alloys, are estimated below. The last term contains the magnetic energy from the magnetic fields, where $\vec{B}_{\rm MS}$ is the magnetostatic field and $\vec{B}_{\rm Oe}$ is the Oersted field.

Using the energy density in Eq. (1), the spin dynamics at $s_1 - s_2 \ll s_1 + s_2$ can be described by the equation for vector $\vec{l}$ only [1,13,18–22]:

$$\frac{s_1 - s_2}{2s_0}\frac{\partial\vec{l}}{\partial t} + \frac{1}{\omega_{\rm ex}}\left[\left(\frac{\partial^2\vec{l}}{\partial^2 t} - c^2\nabla^2\vec{l}\right)\times\vec{l}\right] + \frac{1}{2\hbar s_0}\left(\frac{\delta W_r}{\delta\vec{l}}\times\vec{l}\right) + \alpha_G\left(\frac{\partial\vec{l}}{\partial t}\times\vec{l}\right) + \sigma I\vec{l}\times(\vec{l}\times\hat{\vec{p}}) = 0. \quad (2)$$

Here, W_r is the energy of relativistic interactions, which, in our model, originates from the magnetic field [last term

in Eq. (1)]; $\omega_{\rm ex} = E_{\rm ex}/2s_0\hbar$ is the characteristic exchange frequency; $c^2 = A\omega_{\rm ex}/2s_0\hbar$ is the characteristic velocity that coincides with the spin-wave velocity at $s_1 = s_2$; and $s_0 = (s_1 + s_2)/2$ is the average spin density. Within this approach, the vector $\vec{m}$ or, equivalently, the total spin $\vec{s} = \vec{s}_1 + \vec{s}_2$ is a slave variable and can be present as $\vec{s} = (s_1 - s_2)\vec{l} + 2s_0(\vec{l} \times \partial\vec{l}/\partial t)/\omega_{\rm ex}$, whereas the total magnetization is $\vec{M} = \mu_B[(g_1 - g_2)\vec{l} + (g_1 + g_2)\vec{m}]s_0$. For ferrimagnets such as Gd(Fe, Co) $g_1 - g_2 \sim 0.2$ and the first term of equation for $\vec{M}$ is dominant. The last two terms determine nonconservative dynamics, including Gilbert damping with constant α_G (this constant is quite low: $\alpha_G = 0.007$ for Gd(Fe, Co) alloys [23]), and the last term defines the spin torque from the spin current with polarization $\hat{\vec{p}}$, $\sigma = \varepsilon/(2es_0\pi R^2 L)$, where I is the charge current, ε is the spin-polarization efficiency, e is the magnitude of the electric charge, and πR^2 is the area of the circular nanocontact [24,25].

It is extremely important to note that the spin torque in magnets, such as antiferromagnets or nearly compensated ferrimagnets, is proportional to the vector $\vec{l}$, rather than the total spin [21]; thus, it is finite, even at full compensation. Notably, exactly at the compensation of spins ($s_1 = s_2$), Eq. (2) coincides with the relativistic sigma-model equation, with c as the chosen velocity, and the presence of this Lorentz invariance significantly simplifies the analysis of soliton dynamics (see a recent review, Ref. [26]). In the following, the second time derivative in Eq. (2) is significant near the compensation point, where $(s_1 - s_2)/2s_0 \le \omega/\omega_{\rm ex} \ll 1$ and $\omega/\omega_{\rm ex} \sim 10^{-2}$, which is the case considered here (see the next section).

Magnetization is driven by spin torque in a spin-valve nanopillar structure, where the spin current is polarized in a fixed layer, with magnetization perpendicular to the plane and collinear to the direction of the electron current, as seen in Fig. 1. Vortex dynamics can be described in collective coordinates by transforming Eq. (2) to the generalized Thiele equation [27] for a vortex confined to a magnetic disk, with the vortex core at $\vec{R}_0$ relative to the disk center,

$$M\frac{d^2\vec{R}_0}{dt^2} + \vec{G} \times \frac{d\vec{R}_0}{dt} - \vec{F}_{\rm MS} - \vec{F}_{\rm Oe} = -D\frac{d\vec{R}_0}{dt} + \sigma\hbar L I s_0(\hat{\vec{z}} \times \vec{R}_0), \tag{3}$$

where M is the vortex effective mass, $\vec{F}_{\rm MS}$ is the magnetostatic restoring force, and $\vec{F}_{\rm Oe}$ is the restoring force from the Oersted field. The right-hand side contains the nonconservative spin-torque antidamping force and the Gilbert damping force, which can be taken in the same form as that for the ferromagnetic vortex [28], where the polarization of the current, $\hat{\vec{p}}$, is perpendicular to the disk plane. The Gilbert damping coefficient is $D = \pi\alpha_G\mu_0 M_0^2 L/f_M[\ln(R/2l_{\rm ex}) + 3/4]$, where M_0 is an average of the two magnetizations and $f_M = 2M_0\gamma$ is a characteristic frequency. For a typical ferromagnet, the mass is negligible, but it appears naturally for Eq. (3) with second time derivatives. Moreover, close to the compensation point, the gyrovector, $\vec{G} = \hat{\vec{z}}2\pi\hbar L(s_1 - s_2)$, becomes small, so it is necessary to include a higher time derivative term in the Thiele equation containing the vortex acceleration [1,13].

Next, the terms in Eq. (3) are specified for the two-sublattice model. The effective mass of a vortex in a disk of radius R and thickness L is given in terms of the vortex energy and the spin-wave velocity, c, by $Mc^2 = E_v$, where exchange [29] is the dominant contribution to the vortex energy. To proceed, it is necessary to estimate the constant of uniform exchange between Fe and Gd (the concentration of Co is negligibly small), which can be written as $\varepsilon_{\rm Gd-Fe}\vec{S}_{\rm Gd} \cdot \vec{S}_{\rm Fe}/2$ per single spin, where $\vec{S}_{\rm Gd}$ and $\vec{S}_{\rm Fe}$ are unit vectors parallel to the sublattice spin densities [25,26], $\vec{S}_{\rm Fe} = \vec{m} + \vec{l}$ and $\vec{S}_{\rm Gd} = \vec{m} - \vec{l}$. Then, the exchange energy density becomes $w_{ex} = \varepsilon_{\rm Gd-Fe}\mathbf{m}^2(n_{\rm Gd} + n_{\rm Fe})$, where $n_{\rm Gd} = s_{\rm Gd}/S_{\rm Gd}$ and $n_{\rm Fe} = s_{\rm Fe}/S_{\rm Fe}$ are atomic densities and atomic spins are $S_{\rm Gd} = 7/2$ and $S_{\rm Fe} = 1$; this gives the value of the parameter from Eq. (1) as $E_{\rm ex} = \varepsilon_{\rm Gd-Fe}(n_{\rm Gd} + n_{\rm Fe})$. Using the known value of Gd − Fe exchange [30–32] for one spin, $\varepsilon_{\rm Gd-Fe} = 4.8 \times 10^{-21}$ J, the exchange energy is $E_{\rm ex} = 3.6 \times 10^8$ J/m^3. From this, the exchange frequency is estimated as $\omega_{\rm ex} = E_{\rm ex}/2s_0\hbar = 3.1 \times 10^{13}$ rad/s, or $f_{\rm ex} = 5$ THz. Next, using the vortex energy and spin-wave speed $c = \sqrt{A\omega_{\rm ex}/2\hbar s_0}$, the vortex mass is

$$M = 2\pi L(\hbar s_0/\omega_{\rm ex})\ln(4R/l_{\rm ex}). \tag{4}$$

For a disk of radius R and thickness L, $l_{\rm ex} = \sqrt{A/\mu_0 M_s^2}$ is the exchange length for a saturation magnetization, $M_s = M_1 - M_2$. The gyrovector is proportional to $s_{\rm Gd} - s_{\rm Fe}$, so at the compensation point $G = 0$, and in the following only this case is considered.

III. VORTEX RESTORING FORCE

The additional terms in the Thiele equation are from restoring forces as the vortex core moves off of the disk center. These are from the formation of magnetostatic charges, as well as the force from the Oersted field when the vortex moves off center, which are obtained for the magnetization $\vec{M} = M_s(\cos\varphi, \sin\varphi)$. First, the magnetostatic restoring force is typically obtained without a magnetostatic edge charge, which is calculated using complex variable methods for the circular disk. In this case, magnetization can be expressed as a function of the complex variable with $t = t_1 + it_2$, where $t_1 = x/R$ and $t_2 = y/R$.

The components of the magnetization are given by

$$m_x + im_y = \frac{2w}{1+\bar{w}w}, \tag{5}$$

where the bar indicates complex conjugation and the exchange energy is minimized by any analytical function, $w(t)$. The next step is to find a less general function that will minimize the MS energy subject to the in-plane constraint of the magnetization. For the vortex distribution, the function w is given by

$$w = \frac{f(t)}{\sqrt{f(t)\bar{f}(t)}}, \tag{6}$$

resulting in the vortex-type structure. Finally, the analytical function [33], $f\,(t)$, describing the vortex with no edge magnetostatic charge is the complex function

$$f(t) = i[t - (a + \bar{a}t^2)], \tag{7}$$

where $a = a_1 + ia_2$ is related to the displacement of the vortex core from the disk center, $t_c = \left(1 - \sqrt{1 - 4\bar{a}a}\right)/2\bar{a}$. Equations (5)–(7) then represent the magnetization for a vortex confined to the circular disk with the vortex center at t_c.

Using this form for magnetization, the magnetostatic energy form vortex core displacement has the quadratic form [29,30] for small R_0/R,

$$W_{\rm MS} = \frac{1}{2}\kappa_{\rm MS}R_0^2, \kappa_{\rm MS} = \frac{20}{9}2\pi\mu_0 M_s^2\frac{L^2}{R} \tag{8}$$

where the saturation magnetization is $M_s = M_{\rm Gd} - M_{\rm Fe}$ near the compensation point.

The Oersted energy is calculated using the magnetization in Eqs. (5)–(7) and the field is from a current, I, perpendicular to the disk plane,

$$W_{\rm Oe} = -L\int \vec{M}\cdot\vec{B}d^2r, \tag{9}$$

where $\vec{B}$ is the Oersted field and the integration is over the disk area. In the following, the field inside a long wire is used, $B = \mu_0 Ir/2\pi R^2$, in the tangential direction. This integral over the disk is done numerically and the Oersted energy is shown in Fig. 2 as a function of the vortex core deviation from the disk center. It is noted that, for small displacements of the vortex center ($R_0R/ < 0.2$), this energy can be estimated analytically by expansion of the magnetization in the small parameter, R_0/R, to obtain,

$$W_{\rm Oe} = \frac{1}{2}\kappa_{\rm Oe}R_0^2, \kappa_{\rm Oe} = \mu_0 M_s I\frac{8}{15}\frac{L}{R}. \tag{10}$$

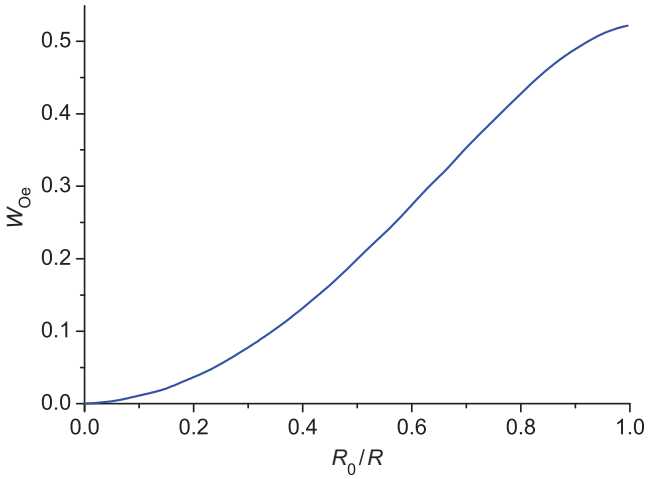

FIG. 2. Oersted energy in units of $\mu_0(M_1 - M_2)ILR$ versus the vortex displacement.

The last two terms in the Thiele equation contain the damping force and spin-torque force, which, for circular orbits, are in the tangential direction and perpendicular to the conservative forces.

IV. SOLUTION OF THE THIELE EQUATION

Now the circular orbit ansatz, $\vec{R}_0 = R_0(\hat{x}\cos\omega t + \hat{y}\sin\omega t)$, is used to solve the Thiele equation, where R_0 is the radius of the gyrotropic orbit. To obtain the frequency, a balance of the radial forces results in

$$M\omega^2 R_0 = F_{\rm MS} + F_{\rm Oe}, \tag{11}$$

where the forces on the right-hand side are the derivatives with respect to R_0 of the corresponding energies at the compensation point ($s_1 = s_2$). In the linear approximation, the frequency is then

$$\omega = \sqrt{\frac{\kappa_{\rm MS} + \kappa_{\rm Oe}}{M}}. \tag{12}$$

For a typical ferromagnet, the effect of the Oersted field on the gyrotropic frequency is small, with $\kappa_{\rm Oe}/\kappa_{\rm MS} \ll 1$, but, for the ferrimagnet, this ratio is $\kappa_{\rm Oe}/\kappa_{\rm MS} = 0.1I/\pi LM_s$ and, especially for small L and M_s, the Oersted restoring force can become dominant.

For nonconservative forces in the tangential direction, it is important to note that dissipation can be compensated for by "antidamping" originating from the spin-pumping effects, resulting in vortex auto-oscillations. From the right-hand side of the Thiele equation [Eq. (3)], the condition of this compensation is $D\omega = \sigma I\hbar Ls_0$, where ω is the frequency of the precessional motion found within the nondissipative approximation. Thus, the threshold value of spin current is obtained from $I_{\rm th} = D\omega/\sigma\hbar Ls_0$,

where the frequency also depends on the current, owing to the Oersted restoring force. Gd(Fe, Co) alloys can have a low Gilbert constant [23], $\alpha_G = 0.007$, and the value of $I_{\rm th}$ is reasonably small, at least for thin disks. The threshold current is obtained numerically using the parameters [21] $M_{\rm Fe} = 10.5 \times 10^5$ A/m, $M_{\rm Gd} = 9.5 \times 10^5$ A/m, and the nonhomogeneous exchange constant [34] of $A = 7.2 \times 10^{-12}$ J/m, to give an exchange length of $l_{\rm ex} = 23.9$ nm. The threshold current density for disks of thickness 3, 3.5, and 4 nm for radii 70–120 nm, with a spin-transfer efficiency of $\varepsilon = 0.3$, is shown as a function of the disk radius in Fig. 3. These current densities correspond to a range of $1.0 \times 10^8 - 3.0 \times 10^8$A/cm^2, which is much higher than that for a typical ferromagnetic vortex-state nanopillar oscillator because of the high oscillation frequency [35,36]. Nevertheless, such high values of current are realized in experiments with standard ferromagnetic active elements to obtain high frequencies in the range 40–60 GHz [37]. Note that contrary to our case, high magnetic fields, such as 1–2 T, were used in Ref. [37]. The gyrotropic frequency versus free-layer radius is calculated from Eq. (12) for the same nanocontact parameters, and these results are illustrated in Fig. 4. First, notice that the frequencies are much higher than that of sub-GHz frequencies of vortex oscillations in ferromagnetic disks. Second, the frequency increases with increasing aspect ratio because of the higher threshold current for larger diameter disks.

From Fig. 3, it is observed that disks with a smaller radius and thickness have lower threshold current densities, so it will be of advantage to use smaller nanopillars. However, there is an aspect ratio limit because of the instability of the vortex of the vortex state and a transition to a single domain state at a critical disk radius. Therefore,

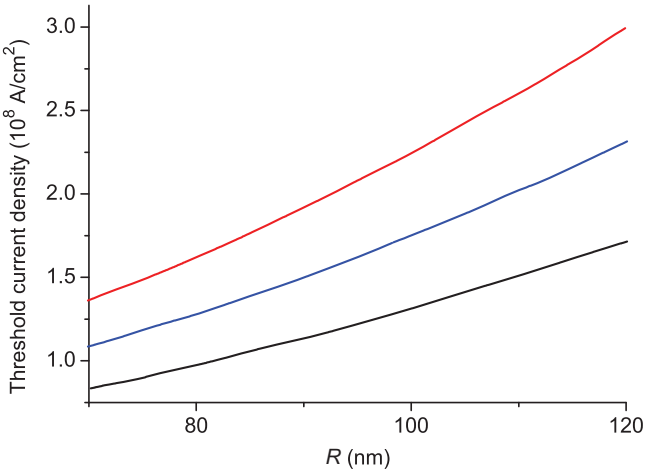

FIG. 3. Threshold current density versus radius for 3, 3.5, and 4-nm thick free layers. Here, and in Figs. 4 and 5, the thinner layer (3 nm thick) corresponds to the lower black curve and the thicker layer (4 nm thick) corresponds to the upper red curve.

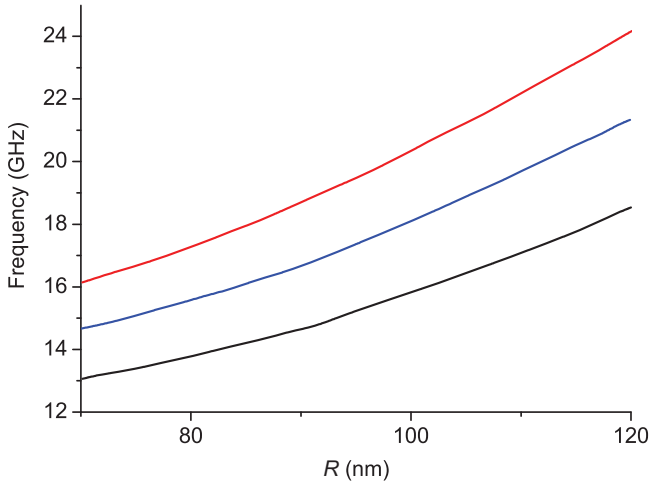

FIG. 4. Gyrotropic frequency versus radius for the 3, 3.5, and 4-nm thick free layer.

the effect of the Oersted field on the stability of the vortex state is considered to obtain a rough estimate of a minimum nanocontact radius. This is done by a comparison of the energies in the single domain state and the vortex state as a function of the nanocontact current. In the single domain state, the energy is mainly of magnetostatic origin, which is expressed as [38]

$$W_{\rm SD} = \mu_0 (M_1 - M_2)^2 \frac{L^2 R}{4} \ln\left(\frac{8R}{L} - \frac{1}{2}\right), \qquad (13)$$

and in the vortex state the energy is mainly a combination of exchange and Oersted energies,

$$W_V = 2\pi A L \ln\frac{R}{l_{\rm ex}} - \mu_0 (M_1 - M_2) I \frac{RL}{3}. \qquad (14)$$

A comparison of these energies for the above parameters, with $R = 70$ and $L = 3$ nm, indicates that they are equal for a nanocontact current of about 15 mA, with a corresponding current density of 10^8 A/cm^2, which is in the region of the critical current density. When the disk radius is increased to 90 nm, these two energies are comparable at a current density of 0.6×10^8 A/cm^2, which is significantly lower than the threshold current density. For this reason, the vortex should be stable for parameters considered in Figs. 3 and 4. Next, the current-dependent frequency is calculated from Eq. (12), using $R = 90$ and $L = 3$ nm, and the results are shown in Fig. 5. Here, it is observed that there is a frequency variation of 180 MHz/mA. For the case of a ferromagnetic nanopillar, the variation of frequency with current is a nonlinear effect, but the variation here is solely the result of the Oersted field. This effect provides an additional frequency-tuning mechanism in ferrimagnetic oscillators. Finally, let us compare the tunability of the ferromagnetic vortex oscillator to the ferrimagnetic

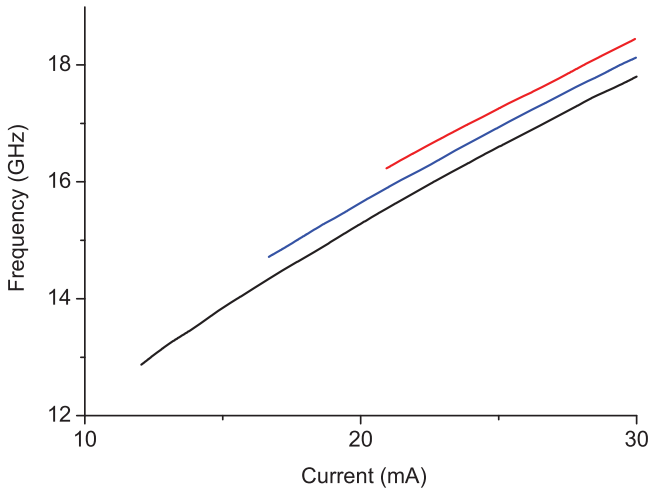

FIG. 5. Gyrotropic frequency versus nanocontact current for 3, 3.5, and 4-nm thick free layers with $R = 70$ nm.

oscillator. From Fig. 5, the slope is estimated to be about 170 MHz/mA and the slope for a ferromagnetic oscillator of the same dimensions is about 10 MHz/mA.

V. CONCLUSION

The ultrafast dynamics of Gd(Fe, Co) alloys is a significant breakthrough in the development of high-frequency nanopillar devices. This is because of significant differences between the ferrimagnetic and ferromagnetic gyrotropic frequencies. First, there is a large frequency difference, as seen by the high frequency for the ferrimagnetic disk, which can be in the range of 15–30 GHz for the above parameters, whereas the ferromagnetic oscillators operate in the sub-GHz range. Second, the Oersted field is more significant, with the benefit that the current can control the frequency over a larger range. This is because the Oersted force is proportional to the small quantity $(M_1 - M_2)$, but the magnetostatic force is proportional to the smaller quantity $(M_1 - M_2)^2$, and contains small multiplier of L/R. In general, the combination of small magnetization and the Oersted field will stabilize the vortex for smaller disk radii, as well as result in much higher oscillation frequencies and significantly increased tunability. Moreover, this generator works with high frequencies (10–20 GHz) without a bias magnetic field that is a mutual consequence of both through exchange enhancement of the spin dynamics in the vicinity of the spin-compensation point of a ferrimagnet [13] and by the action of the Oersted field from the electric current in a nanopillar.

ACKNOWLEDGMENTS

Financial support from the National Academy of Sciences of Ukraine via Project No. 1/17 H; the Program of NUST "MISiS" (Grant No. K2-2019-006), implemented by the Russian Federation governmental decree dated March 16, 2013, No. 211; and by the department of Targeted Training of Taras Shevchenko National University of Kiev at the National Academy of Sciences of Ukraine via project "Elements of ultrafast neuron systems on the basis of antiferromagnetic spintronic nanostructures" is gratefully acknowledged.

[1] S. K. Kim and Y. Tserkovnyak, Fast vortex oscillations in a ferrimagnetic disk near the angular momentum compensation point, Appl. Phys. Lett. **111**, 032401 (2017).
[2] E. G. Galkina, A. Yu. Galkin, B. A. Ivanov, and F. Nori, Magnetic vortex as a ground state for micron-scale antiferromagnetic samples, Phys. Rev. B **81**, 184413 (2010).
[3] S.-B. Choe, Y. Acremann, A. Scholl, A. Bauer, A. Doran, J. Stöhr, and D. C. Padmore, Vortex core-driven magnetization dynamics, Science **304**, 420 (2004).
[4] V. S. Pribiag, I. N. Krivorotov, G. D. Fuchs, P. M. Braganca, O. Ozatay, J. C. Sankey, D. C. Ralph, and R. A. Buhrman, Magnetic vortex oscillator driven by d.c. spin-polarized current, Nat. Phys. **3**, 498 (2007).
[5] R. Lehndorff, D. E. Bürgler, S. Gliga, R. Hertel, P. Grünberg, C. M. Schneider, and Z. Celinski, Magnetization dynamics in spin torque nano-oscillators: Vortex state versus uniform state, Phys. Rev. B **80**, 054412 (2009).
[6] S. Petit-Watelot, J.-V. Kim, A. Ruotolo, R. M. Otxoa, K. Bouzehouane, J. Grollier, A. Vansteenkiste, B. Van de Wiele, V. Cros, and T. Devolder, Commensurability and chaos in magnetic vortex oscillations, Nat. Phys. **8**, 682 (2012).
[7] B. Van Waeyenberge, A. Puzic, H. Stoll, K. W. Chou, T. Tyliszczak, R. Hertel, M. Fähnle, H. Brückl, K. Rott, G. Reiss, I. Neudecker, D. Weiss, C. H. Back, and G. Schütz, Magnetic vortex core reversal by excitation with short bursts of an alternating field, Nature **444**, 461 (2006).
[8] R. P. Cowburn, Spintronics: Change of direction, Nat. Mater. **6**, 255 (2007).
[9] B. Pigeau, G. de Loubens, O. Klein, A. Riegler, F. Lochner, G. Schmidt, L. W. Molenkamp, V. S. Tiberkevich, and A. N. Slavin, A frequency-controlled magnetic vortex memory, Appl. Phys. Lett. **96**, 132506 (2010).
[10] S. Barman, A. Barman, and Y. Otani, Dynamics of 1-D chains of magnetic vortices in response to local and global excitations, IEEE Trans. Magn. **46**, 1342 (2010).
[11] A. D. Belanovsky, N. Locatelli, P. N. Skirdkov, F. Abreu Araujo, K. A. Zvezdin, J. Grollier, V. Cros, and A. K. Zvezdin, Numerical and analytical investigation of the synchronization of dipolarly coupled vortex spin-torque nano-oscillators, Appl. Phys. Lett. **103**, 122405 (2013).
[12] A. V. Khvalkovskiy, J. Grollier, A. Dussaux, K. A. Zvezdin, and V. Cros, Vortex oscillations induced by a spin-polarized current in a magnetic nanopillar: Analytic versus micromagnetic calculations, Phys. Rev. B **80**, 140401(R) (2009).
[13] B. A. Ivanov, Ultrafast spin dynamics and spintronics for ferrimagnets close to the spin compensation point (Review), Low Temp. Phys. **45**, 935 (2019).
[14] D. Houssameddine, U. Ebels, B. Delaët, B. Rodmacq, I. Firastrau, F. Ponthenier, M. Brunet, C. Thirion, J.-P.

Michel, L. Prejbeanu-Buda, M.-C. Cyrille, O. Redon, and B. Dieny, Spin-torque oscillator using a perpendicular polarizer and a planar free layer, Nat. Mater. **6**, 447 (2007).

[15] A. Dussaux, E. Grimaldi, B. Rache Salles, A. S. Jenkins, A. V. Khvalkovskiy, P. Bortolotti, J. Grollier, H. Kubota, A. Fukushima, K. Yakushiji, S. Yuasa, V. Cros, and A. Fert, Large amplitude spin torque vortex oscillations at zero external field using a perpendicular spin polarizer, Appl. Phys. Lett. **105**, 022404 (2014).

[16] T. Okuno, K. J. Kim, T. Tono, S. Kim, T. Moriyama, H. Yoshikawa, A. Tsukamoto, and T. Ono, Temperature dependence of magnetoresistance in GdFeCo/Pt heterostructure, Appl. Phys. Express **9**, 073001 (2016).

[17] A. H. MacDonald and M. Tsoi, Antiferromagnetic metal spintronics, Philos. Trans. R. Soc., A **369**, 3098 (2011).

[18] A. B. Borisov, V. V. Kiseliev, and G. G. Talutz, Solitons in a ferrimagnet, Sol. St. Commun. **44**, 411 (1982).

[19] B. A. Ivanov and A. L. Sukstansky, Nonlinear magnetization waves in ferrites, Zh. Eksp. Teor. Fiz **84**, 370 (1983), [*JETP* 57, 214 (1983)].

[20] B. A. Ivanov and A. L. Sukstansky, Three-dimensional solitons in ferrites and their stability, Solid State Commun. **50**, 523 (1984).

[21] S. K. Kim, K. Nakata, D. Loss, and Y. Tserkovnyak, Tunable Magnonic Thermal Hall Effect in Skyrmion Crystal Phases of Ferrimagnets, Phys. Rev. Lett. **122**, 057204 (2019).

[22] K.-J. Kim, S. K. Kim, Y. Hirata, S.-H. Oh, T. Tono, D.-H. Kim, T. Okuno, W. S. Ham, S. Kim, G. Go, Y. Tserkovnyak, A. Tsukamoto, T. Moriyama, K.-J. Lee, and T. Ono, Fast domain wall motion in the vicinity of the angular momentum compensation temperature of ferrimagnets, Nat. Mater. **16**, 1187 (2017).

[23] D.-H. Kim, T. Okuno, S. K. Kim, S.-H. Oh, T. Nishimura, Y. Hirata, Y. Futakawa, H. Yoshikawa, A. Tsukamoto, Y. Tserkovnyak, Y. Shiota, T. Moriyama, K.-J. Kim, K.-J. Lee, and T. Ono, Low Magnetic Damping of Ferrimagnetic GdFeCo Alloys, Phys. Rev. Lett. **122**, 127203 (2019).

[24] R. Khymyn, I. Lisenkov, V. Tyberkevych, B. A. Ivanov, and A. N. Slavin, Antiferromagnetic THz-frequency Josephson-like oscillator driven by spin current, Sci. Rep. **7**, 43705 (2017).

[25] H. V. Gomonay and V. M. Loktev, Spin transfer and current-induced switching in antiferromagnets, Phys. Rev. B **81**, 144427 (2010).

[26] E. G. Galkina and B. A. Ivanov, Dynamic solitons in antiferromagnets (Review Article), Low Temp. Phys. **44**, 618 (2018)..

[27] A. A. Thiele, Steady-State Motion of Magnetic Domains, Phys. Rev. Lett. **30**, 230 (1973).

[28] B. A. Ivanov and C. E. Zaspel, Excitation of Spin Dynamics by Spin-Polarized Current in Vortex State Magnetic Disks, Phys. Rev. Lett. **99**, 247208 (2007).

[29] K. A. Metlov, Magnetization Patterns in Ferromagnetic Nanoelements as Functions of Complex Variable, Phys. Rev. Lett. **105**, 107201 (2010).

[30] R. F. L. Evans, W. J. Fan, P. Chureemart, T. A. Ostler, M. O. A. Ellis, and R. W. Chantrell, Atomistic spin model simulations of magnetic nanomaterials, J. Phys.: Condens. Matter **26**, 103202 (2014).

[31] T. A. Ostler, R. F. L. Evans, U. Atxitia, O. Chubykalo-Fesenko, I. Radu, R. Abrudan, F. Radu, A. Tsukamoto, A. Itoh, A. Kirilyuk, T. Rasing, and A. Kimel, Crystallographically amorphous ferrimagnetic alloys: Comparing a localized atomistic spin model with experiments, Phys. Rev. B **84**, 024407 (2011).

[32] I. Radu, K. Vahaplar, C. Stamm, T. Kachel, N. Pontius, H. A. Dürr, T. A. Ostler, J. Barker, R. F. L. Evans, R. W. Chantrell, A. Tsukamoto, A. Itoh, A. Kirilyuk, T. Rasing, and A. V. Kimel, Transient ferromagnetic-like state mediating ultrafast reversal of antiferromagnetically coupled spins, Nature **472**, 205 (2011).

[33] K. L. Metlov, Vortex mechanics in planar nanomagnets, Phys. Rev. B **88**, 014427 (2013).

[34] D. Raasch, J. Reck, C. Mathieu, and B. Hillebrands, Exchange stiffness constant and wall energy density of amorphous GdTb-FeCo thin films, J. Appl. Phys. **76**, 1145 (1994).

[35] K. Y. Guslienko, B. A. Ivanov, V. Novosad, Y. Otani, H. Shima, and K. Fukamichi, Eigenfrequencies of vortex state excitations in magnetic submicron-size disks, J. Appl. Phys. **91**, 8037 (2002).

[36] K. Y. Guslienko, X. F. Han, D. J. Keavney, R. Divan, and S. D. Bader, Magnetic Vortex Core Dynamics in Cylindrical Ferromagnetic Dots, Phys. Rev. Lett. **96**, 067205 (2006).

[37] S. Bonetti, P. Muduli, F. Mancoff, and J. Åkerman, Spin torque oscillator frequency versus magnetic field angle: The prospect of operation beyond 65 GHz, Appl. Phys. Lett. **94**, 102507 (2009).

[38] P.-O. Jubert and R. Allenspach, Analytical approach to the single-domain-to-vortex transition in small magnetic disks, Phys. Rev. B **70**, 144402 (2004).